nature chemistry

SUPPLEMENTARY INFORMATION

DOI: 10.1038/NCHEM.2641

Self-assembly of nanoparticles into biomimetic capsid-like nanoshells

Ming Yang[1,2], Henry Chan[3], Gongpu Zhao[4], Joong Hwan Bahng[8,9], Peijun Zhang[4,5*], Petr Král[3,6,7*], Nicholas A. Kotov[1,8,9,10*]

[1]Department of Chemical Engineering, University of Michigan, Ann Arbor, MI 48109, USA;

[2]Key Laboratory of Microsystems and Micronanostructures Manufacturing, Harbin Institute of Technology, Harbin 150080, P. R. China;

[3]Department of Chemistry, University of Illinois in Chicago, Chicago, IL, USA;

[4]Department of Structural Biology, School of Medicine;

[5]Department of Mechanical Engineering and Materials Science, Swanson School of Engineering, University of Pittsburgh, Pittsburgh, PA 15260;

[6]Department of Physics, University of Illinois in Chicago, Chicago, IL;

[7]Department of Biopharmaceutical Sciences, University of Illinois in Chicago, Chicago, IL;

[8]Department of Material Sciences and Engineering, University of Michigan, Ann Arbor, MI 48109;

[9]Departments of Biomedical Engineering, University of Michigan, Ann Arbor, MI 48109;

[10]Biointerfaces Institute, University of Michigan, Ann Arbor, MI 48109.

*E-mail: pez7@pitt.edu, pkral@uic.edu, kotov@umich.edu

INDEX FOR SUPPLEMENTARY INFORMATION:

Supplementary Methods

Supplementary Figures

Supplementary Notes

Supplementary Video Files

Supplementary References

Supplementary Methods

1. NP models used in molecular dynamics (MD) simulations

Effective charges on the atoms constituting the NP cores were Mulliken charges obtained from *ab-initio* calculations.

Atomic partial charges in model 1:

Cd1	0.60	(Cd with one OH ligand)
Cd2	0.50	(Cd with one H_2O ligand)
Cd1 1	0.90	(Cd with two OH ligands)
Cd1 2	0.80	(Cd with one OH ligand and one H_2O ligand)
Cd22	0.70	(Cd with two H_2O ligands)
SCd	-0.14	(S bonded to the ligand-bounded Cd)
SH	-0.47	(S on the NP vertices, capped by H)
Cd	1.17	(bulk, the rest of the Cd in the NP core)
S	-1.17	(bulk, the rest of the S in the NP core)
O1	-1.26, H1 0.46	(OH ligands)
O2	-1.05, H2 0.59	(H_2O ligands)
HS	0.18	

Atomic partial charges in model 2 and 3:

Cd	0.80	(all Cd, NP core and ligands)
S1	0.15	(S with 1 bond, on NP vertices)
S2	-0.37	(S with 2 bonds, on NP edges)
S3	-0.72	(S with 3 bonds, on NP facets)
S4	-0.80	(S with 4 bonds, bulk)
O	-1.32, H 0.32	(ligands in Model 1, based on –OH group in CHARMM)

Variable coordination of the cadmium atoms on the surface of CdS must be taken into account in our system. Two types of surface ligands, for example, OH^- and H_2O, are to be included in simulations, however, their exact distribution over the surface and coordination with the atoms of the NP core is not known. Moreover, the coordination of water and hydroxyl groups to the surface of CdS is expected to be dynamic and vary depending on the local conditions. These difficulties

in assigning a distinct atomic structure in the traditional chemical sense to some of the simplest NPs, and computational difficulties in obtaining long simulations of NPs diffusing in the media, prompted us to model NPs in different ways described **Models 1, 2,** and **3.**

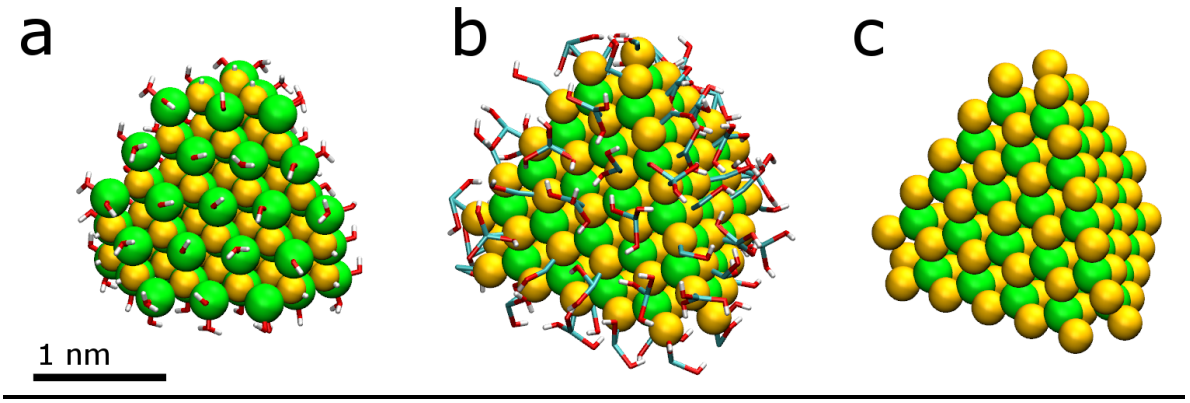

Supplementary Figure 1. Structural representation of NPs in (a) **Model 1** carrying H_2O, OH^-, and H^+ surface ligands typical for neutral and slightly acidic media, (b) **Model 2** carrying OH^-, $Cd(OH)^+$, $Cd(OH)_2$, and $Cd(OH)_3^-$ surface ligands typical for basic aqueous media, (c) **Model 3** carrying no surface ligands. Color coding of the atoms: S - yellow, Cd - green spheres in the NP core and cyan bars in the surface ligands in **Model 2** surface, O - red, and H - white.

Model 1 considered NP 2.4 nm cores with shapes of truncated tetrahedrons that closely matched the constituent NPs. The cores are made from 68 Cd atoms and 52 S atoms that are fully covered by surface ligands typical for a wide range of pH conditions, with H_2O, OH^-, and H^+ corresponding to basic, neutral, and slightly acidic aqueous media. A total of 25 H_2O ligands and 51 OH^- ligands were attached onto each NP to give a net charge of 1.35*e*; the charge is a close match to the experimental value estimated from the zeta-potential measurements. The *ab-initio* calculations of atomic charges were performed for CdS clusters (exemplified by Figure S10 below) in an implicit water environment at the MP2 level, with a 6-31G basis set for H, O, and S atoms,

and LanL2DZ pseudo-potential for Cd atoms, using the Gaussian software.[1] The same *ab initio* calculations were performed for the NP facets, edges, and vertices.

In **Model 2**, we considered NP cores made from 52 Cd atoms and 80 S atoms that are covered by three types of surface ligands: $CdOH^+$, $Cd(OH)_2$, and $Cd(OH)_3^-$. The model assumes the formation of these hydroxyl-derived surface ligands because they are typical for aqueous environment under basic pH conditions used in most experiments. The $CdOH^+$, $Cd(OH)_2$, and $Cd(OH)_3^-$ ligands were randomly distributed on the NP surface, and their ratio was determined by the total NP charge obtained experimentally from zeta-potential values measured using dynamic light scattering (DLS).[2]

Model 3 represents "naked" NP cores identical to **Model 2,** but has no surface ligands. **Model 3** is essential for assessment of surface ligand effects by comparing the results with **Model 2**. In **Models 2** and **3**, the *ab-initio* calculations were performed for the entire NP core in an implicit water environment, using GPU-powered Terachem software[3] at the restricted Hatree-Fock level with a 3-21G basis set.

Models 1, **2**, and **3** are complementary to each other. Each model offers different insights into the effect of surface ligands on NP dynamics and represent a different level of approximation of the system. As the model becomes more atomistically precise, the time window for simulated assembly is narrowed. This set of models represents a combination of conscious compromises between the desire to have the system more accurate and access to longer assembly times.

In **Model 1**, the hydrated NPs interact with each other through multiple hydrogen bonds, bulk vdW attractions, and an electrostatic repulsion. The stabilization of nanoshells is based on the initially proposed physical principles, that is, the balance between vdW, hydrogen attraction, and Coulombic repulsion.

Model 1 allowed us to describe the electrostatic effects of pH and ionic strength on the size of the nanoshell. The time-averaged net charge of the NPs was assigned to sulfur atoms in the NP core, allowing different pH conditions to be modeled while retaining a realistic description of the NP structure and surfaces at an atomic level. The NP assembled nanoshells had average net charges of 0.3*e*, 0.6*e*, and 0.9*e*. These charges matched with those measured experimentally for NPs at different pHs. The exchange of water and ions between the nanoshell cavity and its exterior was simulated for 24–30 ns. The results obtained from **Model 1** matched with those from **Model 2**, indicating that the nanoshells expand as the charge on the NPs increases, which agrees with experimental and heuristic expectations.

In an attempt to show the spontaneous formation of nanoshells in **Model 1**, we simulated the self-assembly of dispersed NPs. Normally, these systems do not have a strong tendency to form aggregated clusters. However, once they are formed, the nanoshells are stable due to a large network of hydrogen bonds. Even large "cracks" do not destroy their integrity. This strong hydrogen bond network is formed because the NPs are rather rigid, so multiple hydrogen bonds between ligands are easily maintained. Although completely formed nanoshells were not observed after 60–90 ns long simulations, we observed the formation of geometrical precursors and components of the nanoshell – NP chains and arc-like portions, depending on the NPs charges.

In **Model 2**, we performed *ab initio* calculations to obtain the atomic Mulliken charge of the whole naked NP core, using restricted Hartree-Fock functions and a 3-21G basis set in TeraChem on GPUs. Using these data, we made assignments of atomic charges to the Cd and S atoms (NP cores) based on the coordination number of atoms, that is, a partial charge of 0.8 for Cd, 0.15 for S with 1 bond (vertices), -0.37 for S with 2 bonds (edges), -0.72 for S with 3 bonds (facets), and -0.8 for S with 4 bonds (NP cores). The atomic charges of the O and H atoms (surface ligands) were taken from hydroxide in the CHARMM force field, which presumably were calculated by *ab initio* methods at the MP2 level.

We found that the simulations using **Model 2** led to NP ligands being interlocked with each other via a collection of strong, attractive intermolecular (vdW and Coulombic) interactions despite the absence of long-distance vdW attractions of the bulk NPs. While fundamentally interesting, these collective interactions caused the NP dynamics to be very sluggish during our simulations: the NP assemblies essentially "froze" in the time scale of atomistic MD. To resolve this problem, we decided to further simplify the model by averaging the atomic charges of the ligands contributing to the net charges placed on the NP cores, while the ligand atoms were not assigned charges. This approach amounts to the partial coarse-graining of the NP-NP interactions and allows to computationally evaluate NP assemblies. This would be difficult to accomplish using a fully atomistic model. Within the approximated **Model 2**, the NP nanoshells were much easier to simulate, allowing us to observe the stability of the nanoshells and the solvent/ion dynamics. We were also able to visualize a partial reorganization of NPs within the preassembled nanoshells.

To better understand the influence of ligand-to-ligand interactions in NP assembly, we carried out simulations using **Model 3,** in which the NPs are "naked". Their cores have the same sizes

and atomic charges as in **Model 2** but their surfaces have no $CdOH^+$, $Cd(OH)_2$, and $Cd(OH)_3^-$ ligands.

In **Model 3**, the atomic charges for the "naked" NPs were calculated in the same way as in **Model 2**, using a restricted Hatree-Fock method with the 3-21G basis set. The only difference was that their values in the MD simulations were reduced by a factor of two to account for the less polar surfaces of NPs carrying the surface ligands.

The explicit core-to-core vdW attraction was also added in **Model 3** to account for the absence of molecular vdW forces between the surface ligands. Because the bulk vdW interactions have a longer range than the 10 Å cutoff distance for non-bonded interactions in our MD simulations, we needed to explicitly add the bulk vdW coupling between NP cores by treating the NPs as spheres with volumes equal to the volume of NPs. The vdW attraction between two spheres is described by

$$V_{ij}^{vdW} = -\frac{A}{12}\left\{\frac{R}{D_{ij}[1+D_{ij}/4R]} + \frac{1}{1+D_{ij}/R+D_{ij}^2/4R^2} + 2\ln\left(\frac{D_{ij}[1+D_{ij}/4R]}{R[1+D_{ij}/R+D_{ij}^2/4R^2]}\right)\right\},$$

where the Hamaker constant is 5.24×10^{-20} J (CdS-CdS in water), R is the radius of interacting spheres, and D_{ij} is their center-to-center distance. A cutoff of 70 Å was used to select neighboring NPs in the evaluation of bulk vdW attractions. The vdW forces between NPs was re-evaluated every 1000 steps (ca. 2 ps) and it was applied to the atom closest to the center of the NP. NPs in this model have weaker coupling, therefore, we consider smaller $q = 0.6e$, $1e$, and $2e$.

Model 3 is a further simplification of **Models 1** and **2.** It allowed us to partially resolve the problem of mismatch between time scales characteristic of atomistic MD simulations and the time scale characteristic of NP reorganization. This change facilitated particle dynamics while retaining

an atomistic description of the NPs. Facilitation of the reorganization dynamics of nanoshells allowed **Model 3** to describe the morphology of the experimental nanoshells more accurately than **Model 2.** Since there are no ligands on the NPs, the dynamics are relatively fast. We even observed the spontaneous formation of pores in the nanoshells, in analogy to the experiments. Interestingly, the bulk NP charges for which the nanoshells could be stabilized in the model are similar to the experiments. **Model 3** with "naked" NPs is also reminiscent of the DLVO model, but it has more realistic solvent dynamics with osmotic and other forces included.

An opening of ~8 nm^2 was created in the nanoshells (prior to the NP charge assignments) by removing two NPs and spatially fixing atoms of the surrounding NP cores, in agreement with the observed porosity of nanoshells. The opening accelerated the free flow of ions and water molecules and led to faster stabilization of the nanoshells.

2. Calculation of Surface Charge of CdS NPs

The total surface charge of CdS NPs, Q_{CdS}, is obtained from the following relations:

$$Q_{CdS} = 4\pi R_{CdS}^2 * \sigma_{CdS},$$

where R_{CdS} is the radius of the CdS NPs and σ_{CdS} is the surface charge density, given by the following:[4]

$$\sigma_{CdS} = \frac{2\varepsilon_r\varepsilon_o\kappa k_B T}{ze}\sinh\left(\frac{ze\psi_{CdS}}{2k_B T}\right)\sqrt{\left[1 + \frac{1}{\kappa R_{CdS}}\frac{2}{\cosh^2(\frac{ze\psi_{CdS}}{4k_B T})} + \frac{1}{(\kappa R_{CdS})^2}\frac{8\ln[\cosh(\frac{ze\psi_{CdS}}{4k_B T})]}{\sinh^2(\frac{ze\psi_{CdS}}{2k_B T})}\right]},$$

where the surface potential ψ_{CdS} assumes the ζ-potential value, ε_0 is the permittivity of vacuum, ε_r is the dielectric constant of water, k_B is the Boltzmann constant, and T is the absolute temperature. The Debye length, κ, is given by,

$$\kappa = \sqrt{\frac{1000 N_A e^2}{\varepsilon_r \varepsilon_0 k_B T} \sum_i M_i \times z_i^2} \quad ,$$

where e is electric charge (Coulomb), N_A is Avogadro's number, M_i and z_i are the molar concentration and valency of ions, respectively.

3. Number of NPs in nanoshells

Using a geometrical model of a hollow sphere with radius *R* comprised of small spheres with radius *r* (Fig. S2a), we may calculate the upper bound of the number of NPs in a nanoshell (*N*). The equators of the small spheres form packing of circles on the hollow sphere of radius *R*. If *R* is much larger than *r*, this is like packing circles in the plane, and the packing is then optimal with a density of $\frac{\pi}{2\sqrt{3}} = 0.9$. We know that the surface area of the hollow sphere is $4\pi R^2$, and the area of the equatorial circles of small spheres is πr^2, then *N* can be calculated as $N = \frac{4\pi R^2 \times 0.9}{\pi r^2} = \frac{3.6R^2}{r^2}$. Using the average diameter of nanoshells (pH = 9.5, *R* = 10 nm) and the average size of NPs (*r* = 2 nm), the aggregation number of NPs, $N_{R=10\,nm}$ can be calculated to be 90.

4. DLVO Model for Nanoshells

Comparison of MD simulations with DLVO model(s) is particularly informative when evaluating different options for an adequate description of large NP assemblies. The equality of the vectorial sum of all repulsive and attractive forces associated with pairs of spherical NPs in a dielectric medium is the criterion for stability of a nanoshell (Fig. S2). One can calculate these forces for a NP located in the pole of the shell and, because of their spherical symmetry, this can be extended to any particle in the assembly. As expected, the number of NPs in a nanoshell is dependent on the average charge of individual NPs, q. The increase of q leads to smaller nanoshells, which may seem counterintuitive because the distances between NPs become smaller. The result originates from the fact that electrostatic interactions dominate in this model and the smaller number of NPs in the nanoshell leads to the smaller integral Coulombic repulsion. However, due to the simplicity of this DLVO model, the formation of pores on the nanoshell might be treated as a point of instability in the model.

The primary interactions between NPs within the constraints of the classical DLVO model are van der Waals (*vdW*) attractions and screened electrostatic repulsions. It is widely accepted practice in DLVO to reduce vdW forces to London dispersion forces (LDFs). The other two components of vdW – the Keesom force between permanent rotating dipoles and the Debye force between a permanent rotating dipole and an induced dipole, could be also present for NPs, but are typically ignored within the classical DLVO framework.

Using spheres as models for NPs, which is common for recent applications of DLVO to nanoscale dispersions,[4,5,6,7,8,9] linearized Poisson-Boltzmann approximation for electrostatic interactions, and Derjaguin approximation for dispersion forces of vdW interactions, the potential energies of these two interactions can be described by Eqs. 1–3

$$U_{PB}(D_{ij}) = \frac{q_i q_j}{4\pi\varepsilon\varepsilon_0 D_{ij}} e^{-\kappa D_{ij}} C_0^2 \quad (1)$$

$$C_0 = \frac{e^{\kappa r}}{1+\kappa r} \quad (2)$$

$$U_{vdW}(D_{ij}) = -\frac{Ar}{12D_{ij}} \quad (3)$$

Here, q_i and q_j are the net charges carried by NP_i and each NP in the j circles (NP_j) (j = 1, 2, 3……$\frac{N_e}{2}$), N_e is the number of NPs in the equatorial circle, D_{ij} is the center-to-center distance between constituent NPs designated as i and j, $1/\kappa$ is the Debye screening length which is estimated based on the ionic concentrations, r is the average radius of NPs, ε_0 is the permittivity of the vacuum, ε is the effective permittivity of the solvent (water), A is Hamaker constant of CdS-water-CdS, which is 4.9×10^{-20} J, T is the temperature of this self-assembling system; in our experiments, T = 298 K.

Assuming that all Cd^{2+} ions are consumed and form CdS, because thioacetamide is present in excess, only monovalent ions are present in the solution. The main types of ions are ClO_4^-, CH_3COO^-, and Na^+. Although other positive ions such as NH_4^+ may exist, we can use the concentrations of ClO_4^- and CH_3COO^- to estimate the ionic strength (I) taking advantage of the law of electrical neutrality. The concentration of ClO_4^- (0.0004 M) was calculated based on the initial amount of $Cd(ClO_4)_2$ and the concentration of CH_3COO^- (0.0004 M) was calculated based on the initial amount of thioacetamide, assuming that all thioacetamide is transformed into CH_3COO^- at pH 9.2. Note that acetate ion has minimal affinity to the surface of CdS, especially compared to abundant water molecules and OH^- groups; it will not form an organic coating on the NPs. The overall concentration of positive ions is 0.0008 M, which is necessary to electrically neutralize the solution. I can be calculated according to the following equation:

$$I = \frac{1}{2}\sum_{i=1}^{n} c_i z_i^2,$$

where c_i is the molar concentration of ion i (M), z_i is the charge number of that ion, and the sum is taken over all ions in the solution. I was then estimated to be 0.0008 M. At room temperature (25 °C), for 1:1 electrolytes in water, we have

$$\kappa^{-1}(nm) = \frac{0.304}{\sqrt{I(M)}} = \frac{0.304}{\sqrt{0.0008}} \approx 10\ nm,$$

The coexistence of attractive vdW and repulsive electrostatic forces with different characteristic range under certain circumstances, according to DLVO theory, can indeed produce stable nanoshells. Taking the derivatives of potential energies U with respect to D_{ij} allows us to establish the balance of forces acting on each NP:

$$\vec{F}_{PB} = -\frac{d\left[U_{PB}(D_{ij})\right]}{d(D_{ij})} = -\frac{q_i q_j}{4\pi\varepsilon\varepsilon_0}\frac{d\left({D_{ij}}^{-1}e^{-kD_{ij}}\right)}{d(D_{ij})} = \frac{q_i q_j}{4\pi\varepsilon\varepsilon_0}\left(\frac{\kappa e^{-kD_{ij}}}{D_{ij}} + \frac{e^{-kD_{ij}}}{{D_{ij}}^2}\right)$$
$$= \frac{q_i q_j}{8.73\times10^{-9}}\left(\frac{10^8}{D_{ij}\times e^{10^8\times D_{ij}}} + \frac{1}{D_{ij}^2\times e^{10^8\times D_{ij}}}\right) \quad (4)$$

$$\vec{F}_{vdW} = -\frac{d\left[U_{vdW}(D_{ij})\right]}{d(D_{ij})} = -\frac{Ar}{12D_{ij}^2} \quad (5)$$

One can evaluate the stability of the nanoshells in terms of repulsive and attractive forces acting on the NP$_i$ located in the pole of the nanoshell (Fig. S2a,b). Note that the force analysis is simpler. Also, analytical expressions for pair interactions in terms of the total energy (enthalpy) must involve special precautions, avoiding a double count of the energy of NP$_i$-NP$_j$ and NP$_j$–NP$_i$ pairs, which are the same. The absolute value of F_{vdW} and F_{PB} are the same for all the particles within the latitudinal circle at the distance D_{ij} from NP$_i$ located in the pole of the nanoshells. Adhering to the core postulates of DLVO, let us assume for simplicity of calculation that these interactions are additive. Then the requirement for the stable nanoshell will be equality of the vectorial sum of all repulsive and attractive forces associated with NP pairs:

$$\vec{F}_{repulsion} = \sum_{j=1}^{\frac{Ne}{2}} n_j \vec{F}_{PB} \sin\frac{\theta}{2} \quad (6)$$

$$\vec{F}_{attraction} = \sum_{j=1} n_j \vec{F}_{vdW} \sin\frac{\theta}{2} \qquad (7)$$

$$\vec{F}_{repulsion} + \vec{F}_{attraction} = 0 \qquad (8)$$

where N_e is the number of NPs in the equatorial circle of the nanoshell, n_j is the number of NPs in the j circle, and angle θ is described in Fig. S2a,b. Due to the spherical symmetry and identity of all the constitutive NPs in the nanoshell model, the analysis for NPs in the poles of the nanoshells can be extended to all NPs in the assembly. Note that we only account for the attractive vdW forces between the polar particles and their immediate neighbors which is in line with the MD simulations described above.

Now one can infer that

$$D_{ij} = \frac{2r\sin\frac{\pi j}{N_e}}{\sin\frac{\pi}{N_e}} \qquad (9)$$

$$\theta = \frac{2\pi j}{N_e} \qquad (10)$$

$$n_j = \frac{\pi}{\sin^{-1}\left(\frac{\sin\frac{\pi}{N_e}}{\sin\frac{2\pi j}{N_e}}\right)} \qquad (11)$$

The number of NPs in a nanoshell, N, is dependent on N_e as

$$N = 1 + \sum_{j=1}^{\frac{N_e}{2}} n_j \qquad (12)$$

Combining Eqs. 4–11 and assuming that the electrical charges carried by NP_i and NP_j are the same and equal to an ensemble-averaged, that is, $q = q_i = q_j$, we can see that by assigning a series of integers to N_e we can get the corresponding values of q based on Eqs. 6–11. N can be calculated based on N_e according to Eq.12. A plot of N vs. q is given in Fig. S2c. Similarly, by treating q as a variable, a plot of N vs. I can be obtained (Fig. S2d).

Note that when advanced versions of DLVO with improved parametrization of NP interactions including, for instance, dependence of Hamaker constant particle size[9] or special consideration for steric repulsion,[6] the form of the Eqs. will change. However, all of the key assumptions put in foundation of DLVO, especially the mean field approximation of electrostatic interactions represented by Eqs. 1, 2, and 4, will not.

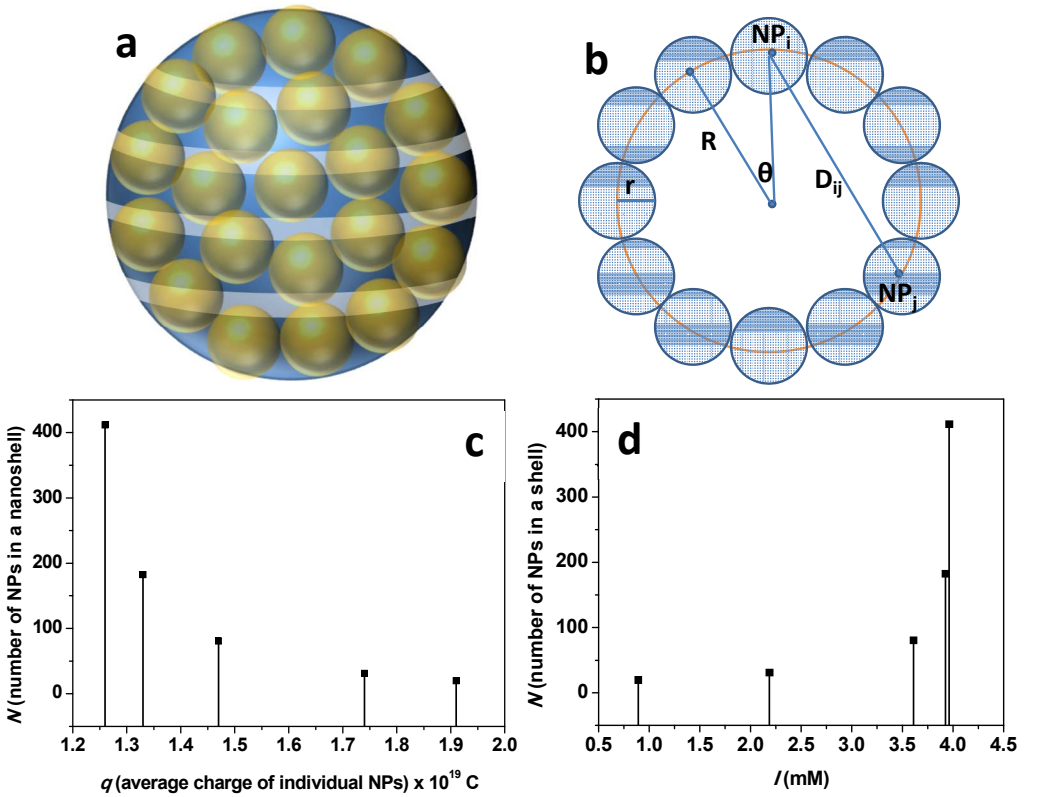

Supplementary Figure 2. Schematic illustration of the model used for DLVO calculations: (a) side view, (b) cross-sectional view. (c) Dependence of the number of NPs in a nanoshell, *N,* on average NP charge, *q*. (d) Dependence of the number of NPs in a nanoshell, *N*, on the ionic strength, *I*, with a fixed *q* (1.91×10^{-19} C).

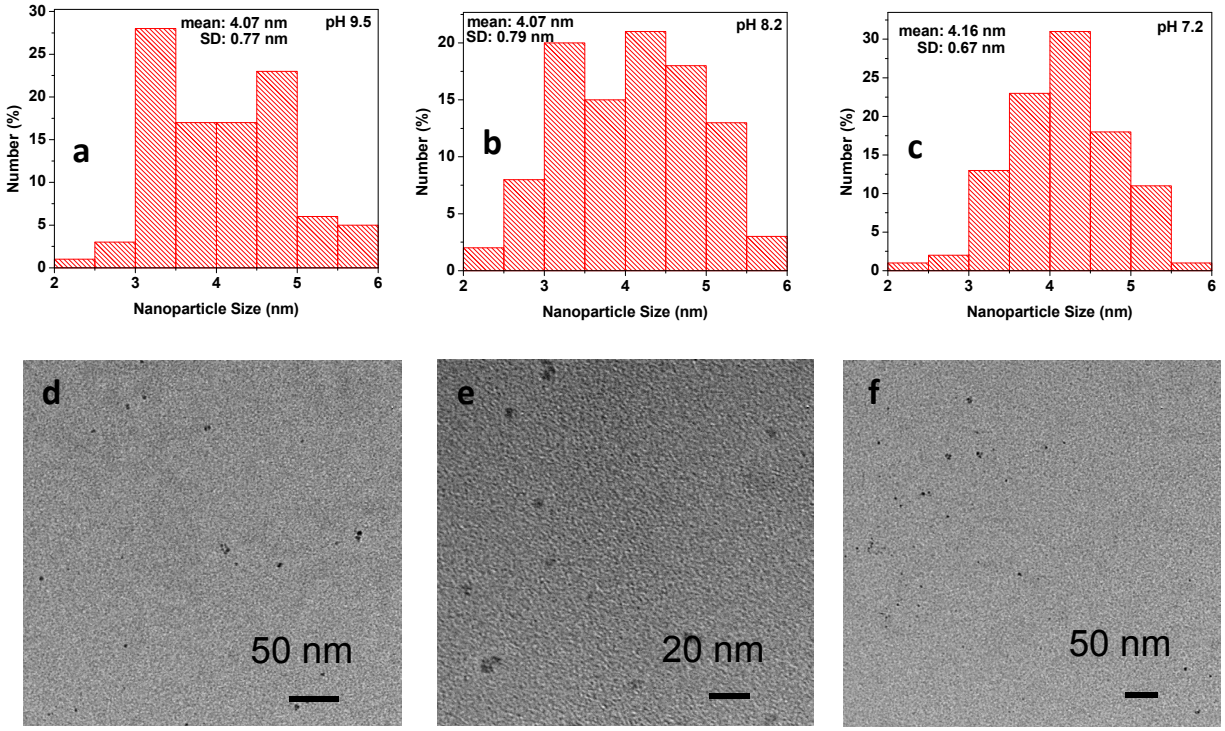

Supplementary Figure 3. (a-c) Size distributions of constituent NPs after 5 min reaction under different pH conditions of 9.5, 8.2, and 7.2. For each graph, 100 NPs from TEM images were measured. (d-f) TEM images of NPs obtained after 5 min reaction under different pH conditions of 9.5, 8.2, and 7.2.

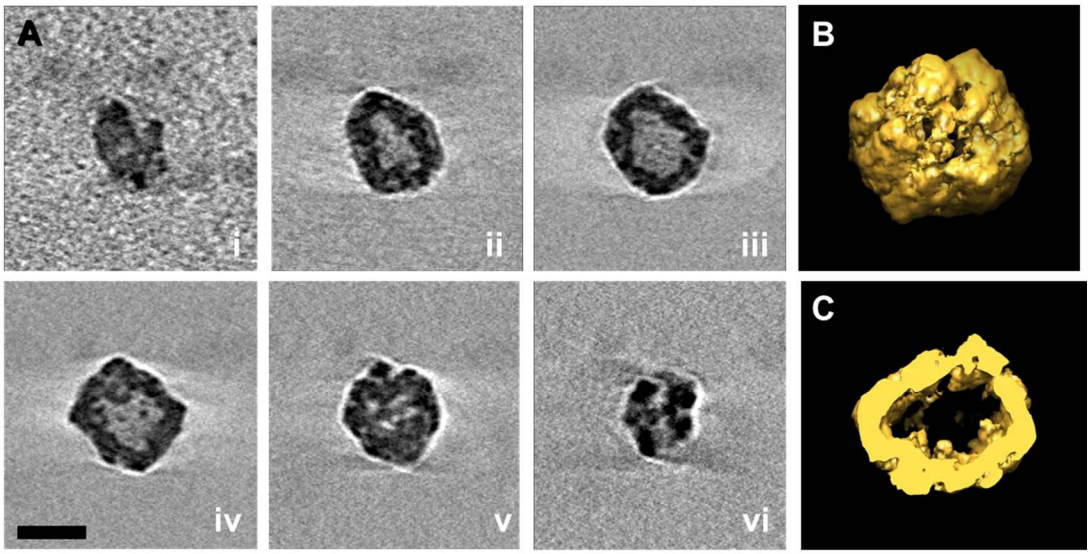

Supplementary Figure 4. Room temperature tomographic reconstruction of a CdS nanoshell. (A) *X*-*Y* slices (i-vi) reconstructed from a 3D tomography of a CdS nanoshell, shown in every 4.5 nm through the volume. Scale bar is 20 nm. (B) 3D surface rendering of the nanoshell. (C) Cross-section of the nanoshell.

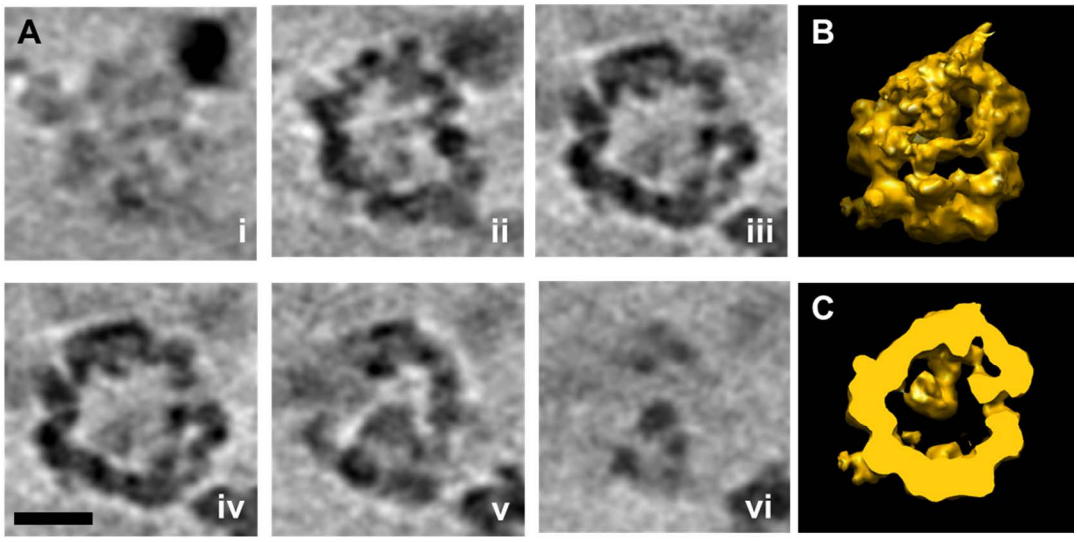

Supplementary Figure 5. Cryo-electron tomographic reconstruction of a CdS nanoshell. (A) *X-Y* slices (i-vi) reconstructed from a 3D cryo-electron tomography of a CdS nanoshell, shown in every 3 nm through the volume. Scale bar is 10 nm. (B) 3D surface rendering of the nanoshell. (C) Tomographic reconstruction of the cross-section of the nanoshell.

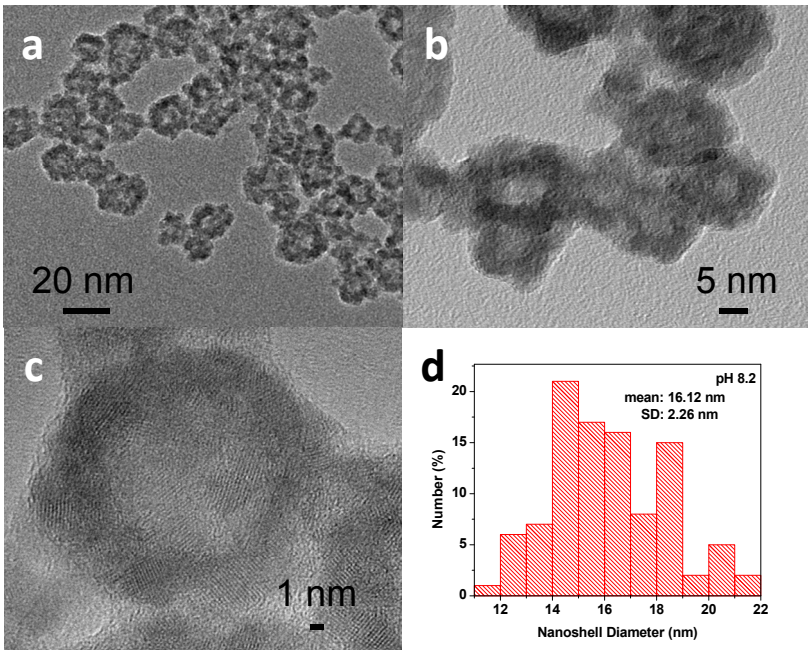

Supplementary Figure 6. (a-c) TEM images of NP assemblies obtained at pH 8.2. (d) The size distribution of nanoshells obtained at pH 8.2.

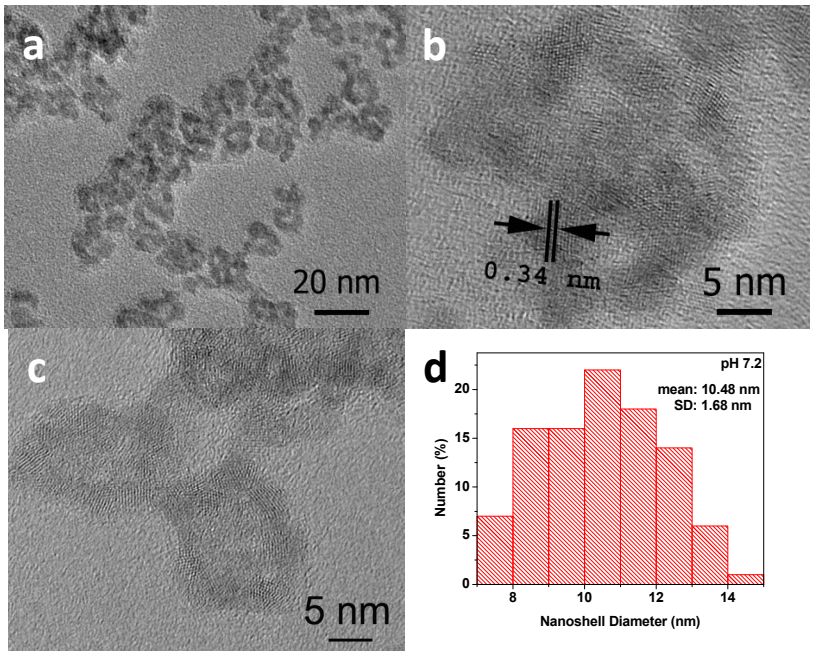

Supplementary Figure 7. (a-c) TEM images of NP assemblies obtained at pH 7.2. (d) The size distribution of nanoshells obtained at pH 7.2.

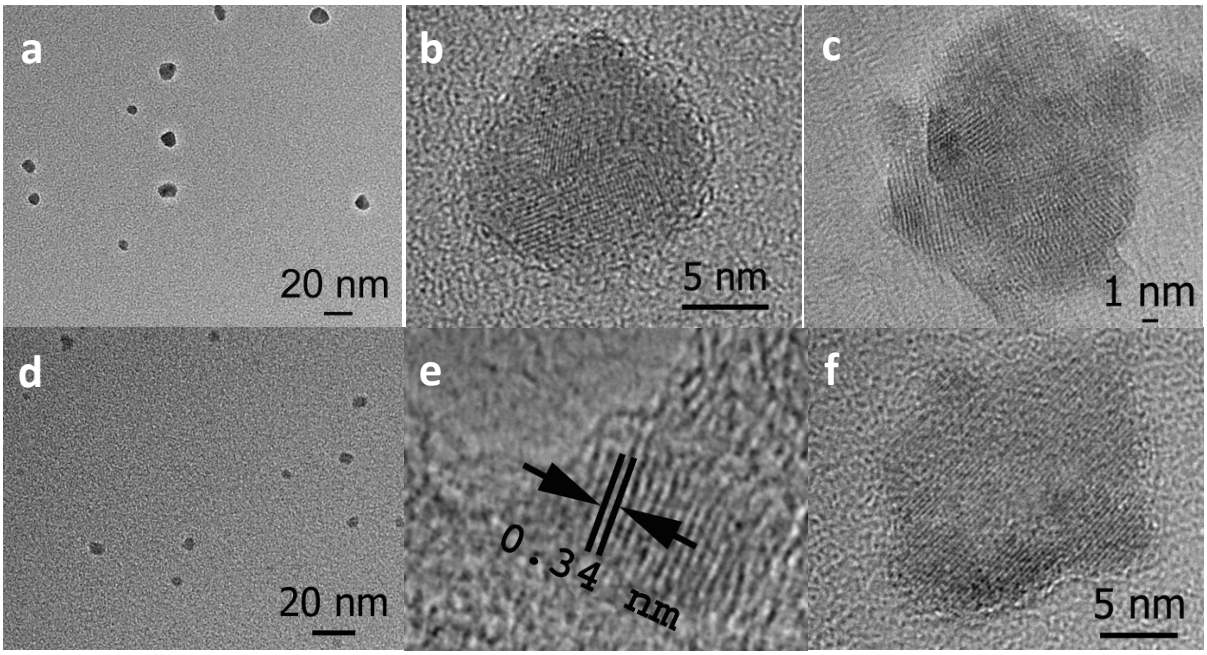

Supplementary Figure 8. TEM images of NP assemblies obtained at (a-c) pH 5 and (d-f) pH 4.3.

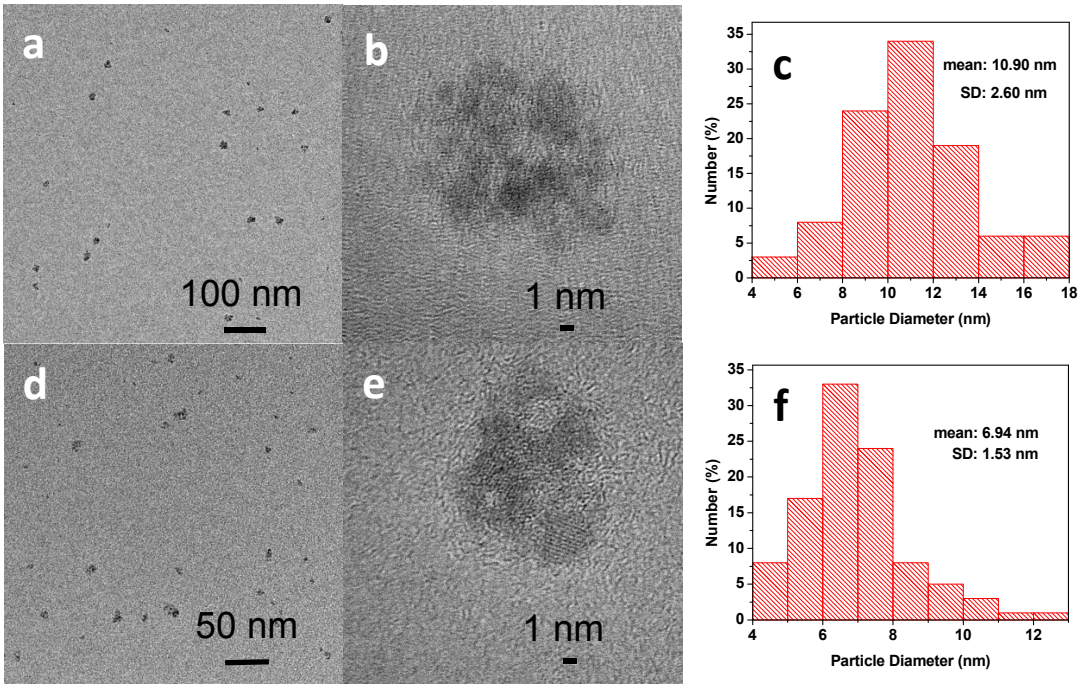

Supplementary Figure 9. TEM images and size distributions of NP assemblies obtained at ionic strength of (a-c) 5.8 mM and (d-f) 10.8 mM, respectively. The ionic strength was controlled by adding NaCl. The size distribution was obtained by measuring the diameters of 100 particles.

(a)

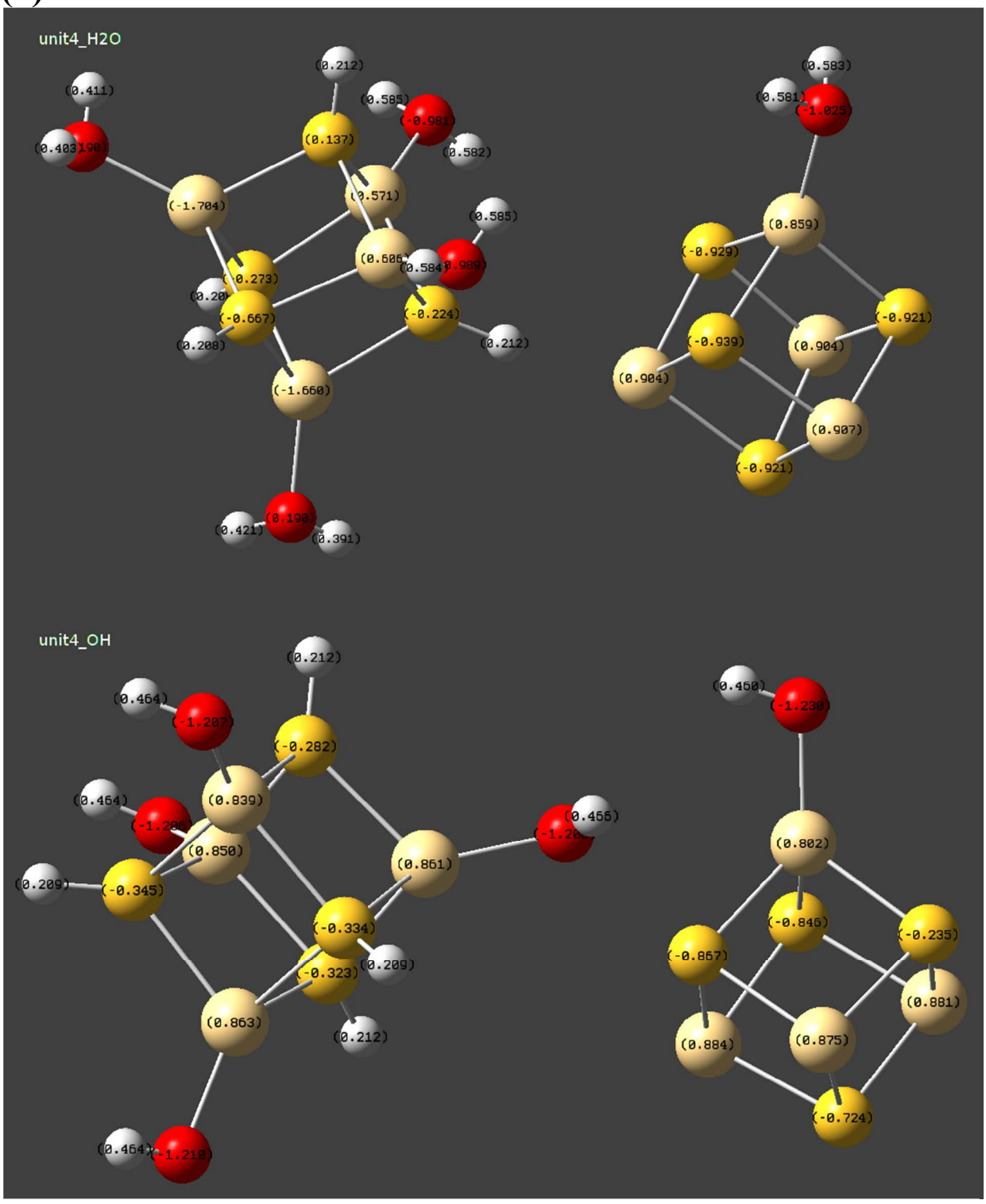

(b)

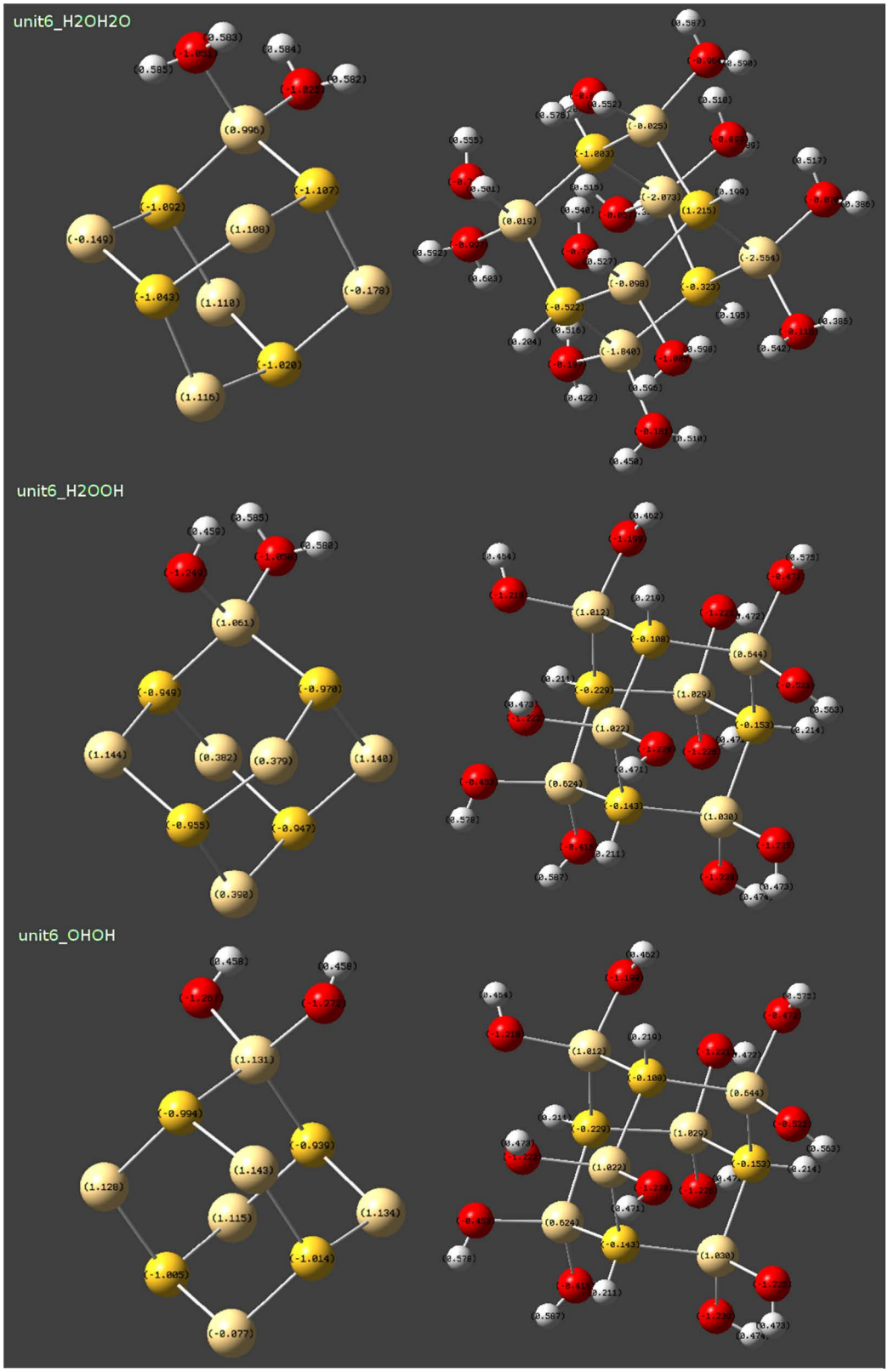

(c)

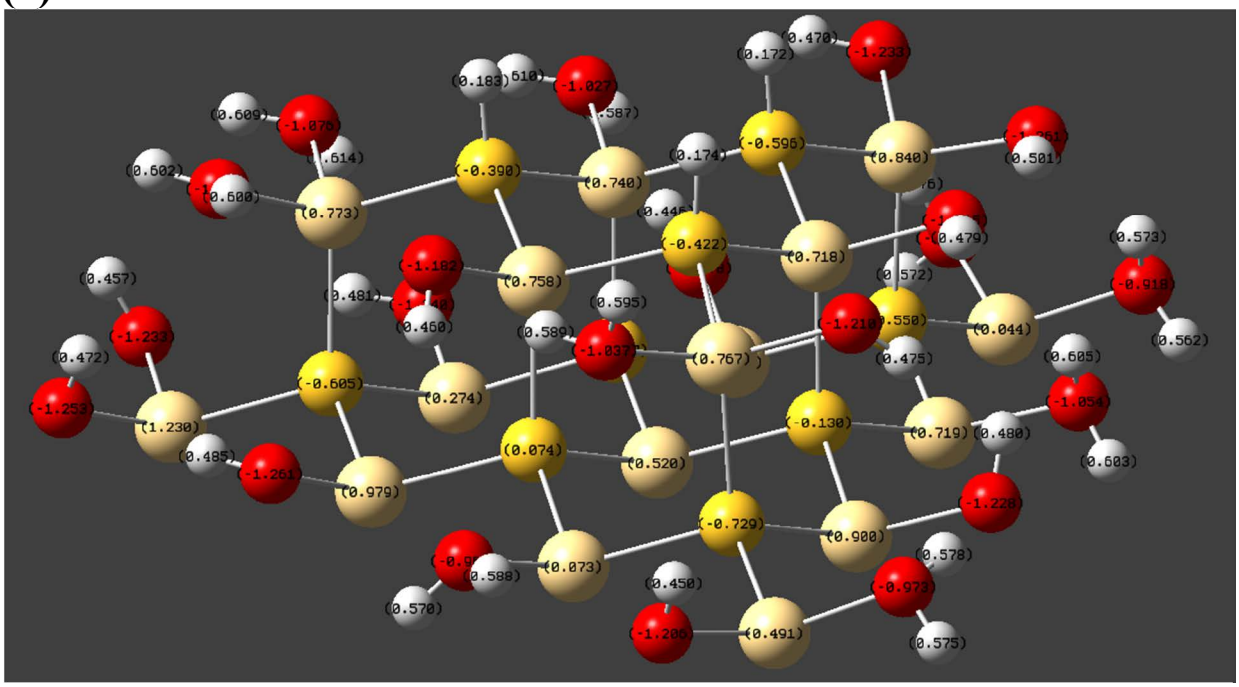

(d)

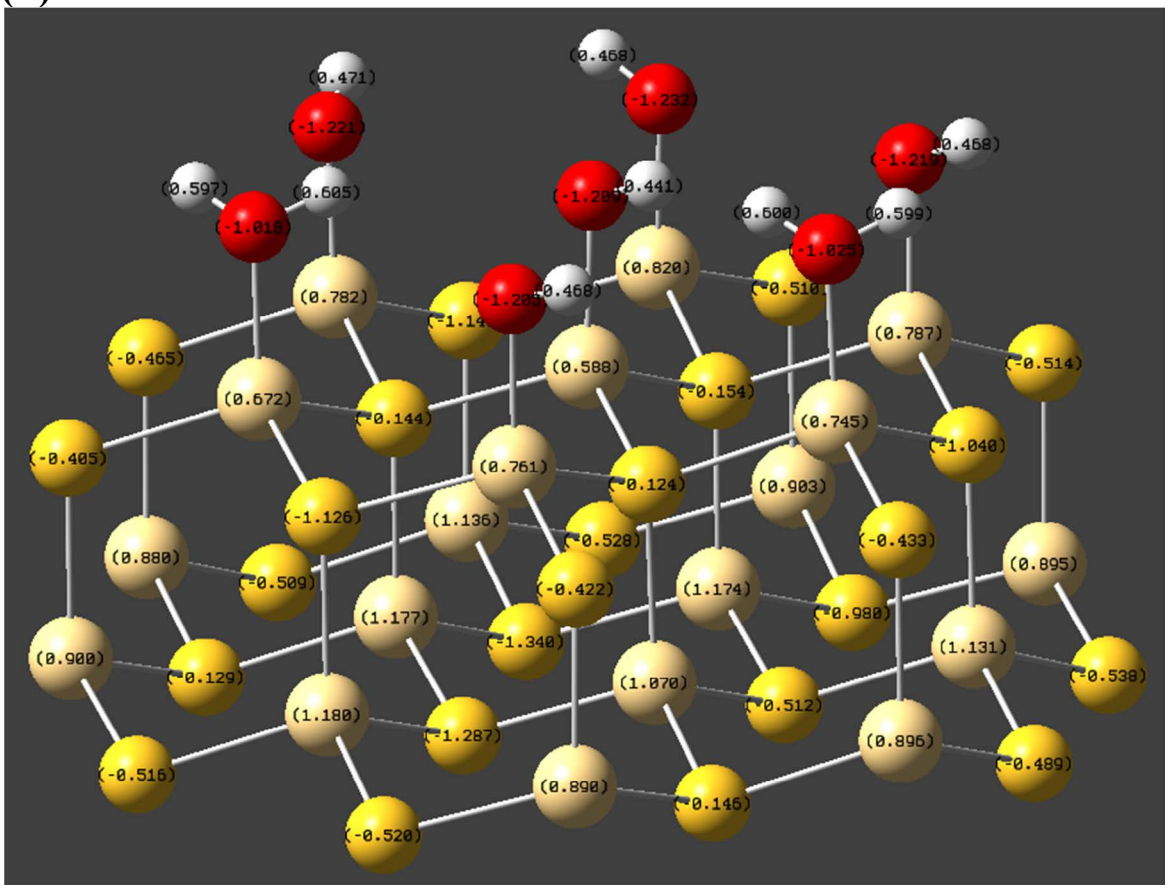

(e)

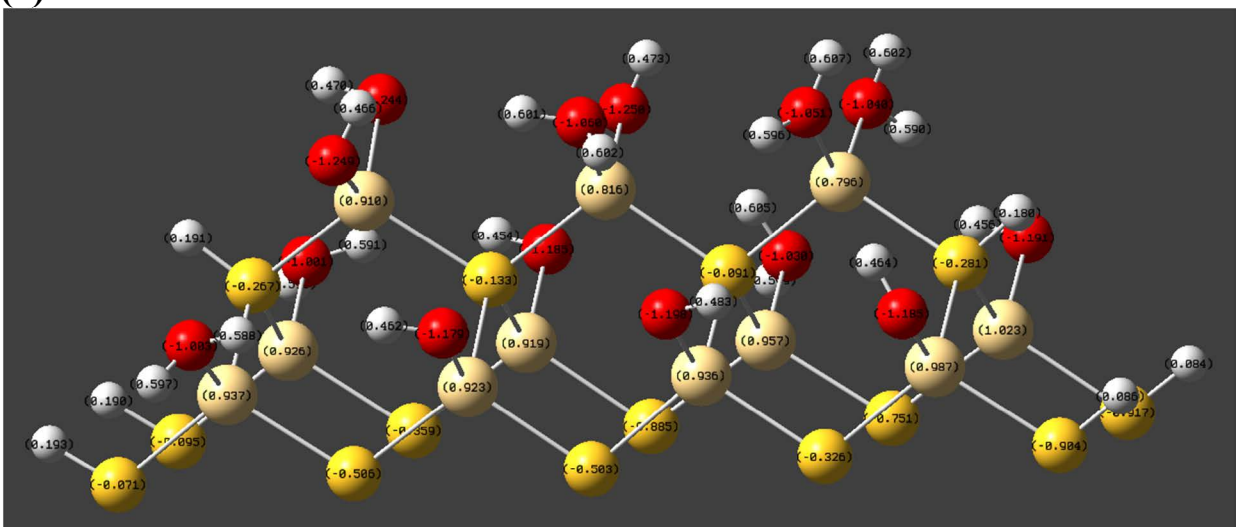

Supplementary Figure 10. Reference atomic charges for **Model 1** obtained from Gaussian calculations performed at the MP2 level using 6-31G basis set for H, O, S atoms, LanL2DZ pseudo-potential for Cd atoms, and in implicit water environment. (a-b) Small CdS clusters with OH^- and H_2O ligands. (c) Corner of a NP. (d) Face facet of a NP. (e) Edge of a NP.

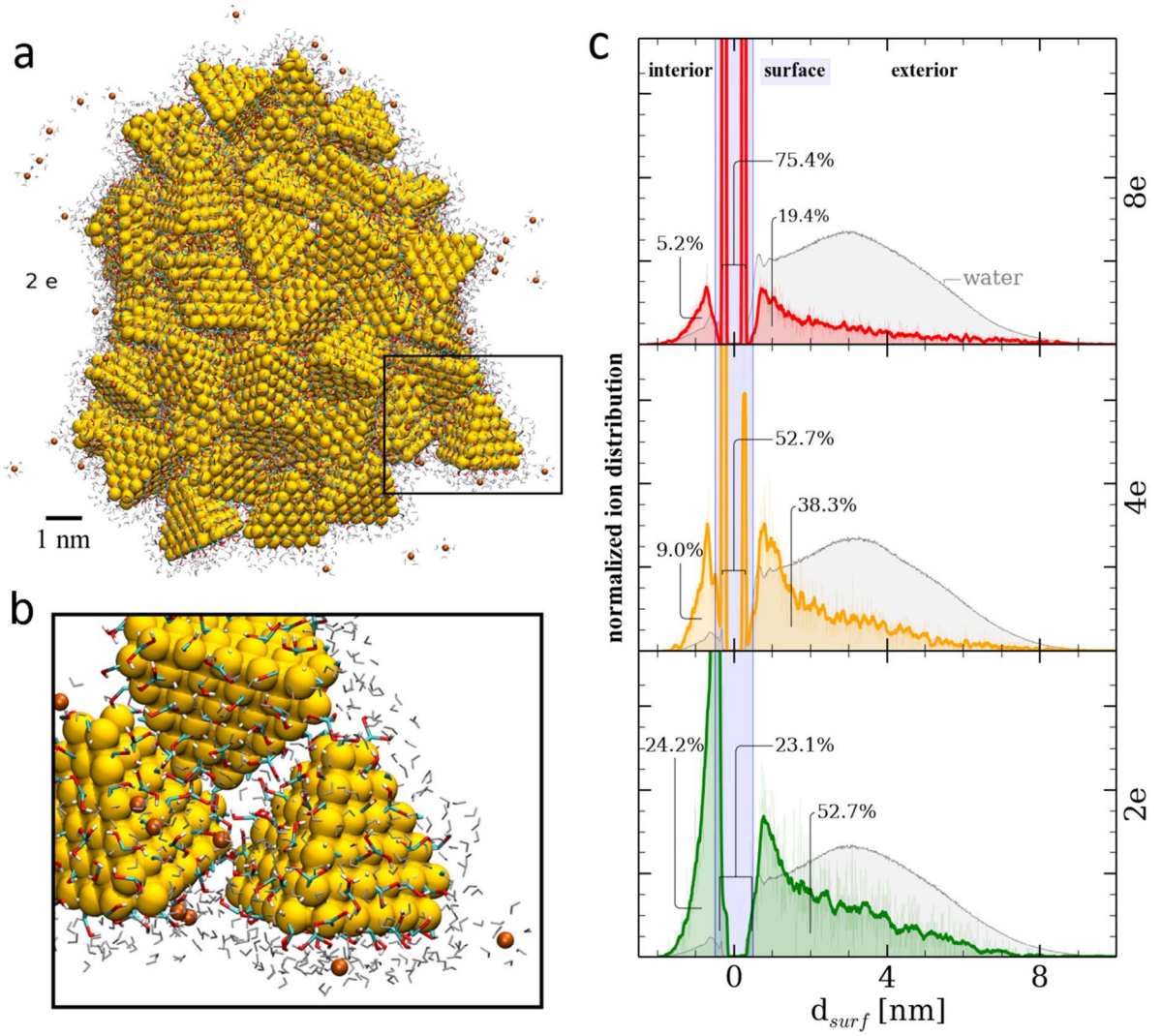

Supplementary Figure 11. (a) Snapshots of nanoshell formed by NPs in **Model 2** carrying net charge $q = 2e$. (b) An enlarged view of the highlighted region. (c) Distribution of ion inside (negative d_{surf}) and outside (positive d_{surf}) of the nanoshells. d_{surf} is the distance from the surface of the NP cores.

Supplementary Note 1: Previous Nanoparticle studies combining electron microscopy data and simulations.

Although a lot of progress has been made over the past 15 years in computer descriptions of NPs and their assemblies, there is still much to accomplish. Early on, simple Monte-Carlo methods described NPs as spheres in a 2D plane were able to show the formation of chains from dipolar NPs.[10,4,11,12] Later, more sophisticated 3D methods with geometrically accurate coarse-grained NPs showed the formation of hexagonally closely packed assemblies,[13] Wulff polyhedra,[14] sheets,[15] and twisted ribbons.[16] Now the simulations can be carried out on an atomistic scale with similar 3D TEM images to match demonstrating sophisticated superstructures.[17]

In the past several years, literature indicates that atomistic MD simulations (25k – 2 million atoms and ps and ns time scale) have been used to model experimental nanoscale objects, but none of them attempted the atomistic simulation of multiple NPs in atomistic media for the time sufficient for self-assembly of NPs in complex multi-unit objects. They all have distinct differences with the present work, and adequate MD and other modeling of NP processes remains a challenge.

Most of the studies integrating MD simulations with TEM data essential in the framework of this project use simulations that connect *dynamics of atomic structure within singular NPs* whose crystal lattice is visualized by TEM.[18–25]

Modeling of a single NP by short-range reactive force fields pursues a different research goal and is limited to processes relevant to molecular oscillations for chemical reactions on the NP surface. Our study differs from other studies in that we focused on the self-assembly and structural formations of *multiple NPs in an aqueous environment that is also described atomistically*. As

we expressed above, having longer effective time of simulations is essential for such systems, but must also include both short- and long-range interactions.

Among these other studies, the papers by Ascencio *et al*. focused on bimetallic Au/Cu NPs[18], a paper by Fan *et al*. about CdSe NPs,[21] and a paper by Chen *et al*. on Cu NPs[26] could be particularly representative. They showed atomistic MD simulations of the dynamical structural transformation of NPs into core-shell NPs, tetrapods (~400 K – 1200 K), and melting of Cu NPs (1052 K) under vacuum. These studies showed agreement with structures observed in TEM data but they are all focused on the changes of the crystal lattice of the *individual* NPs.

Another study with relevance our work is the paper by Zhang *et al.,* which described the combination of advanced TEM analysis coupled with MD simulations of NP dimers bridged by DNA oligomers.[25] Note that only the DNA section of this assembly was modelled with atomistic precision while the total time window of simulations was within the 100 ps range.

Our study of self-assembly of CdS NPs includes rich chemistry of surfaces and their self-assembly occurs in aqueous solution. Moreover, the TEM data are different in our case, because we made the comparison with the *three-dimensional TEM data of multiple NP units*.

This work made a step forward by developing adequate models for describing dynamics of large NP systems affording a partial account of the non-additivity of NP-NP interactions.[27] However, considering the difficulties of simulating the slow dynamics using an atomistic model, further theoretical and computational descriptions of NP systems are still needed.

Supplementary Note 2: Osmotic forces

The studies using **Model 2** demonstrate that the number of ions inside the equilibrated nanoshells has a tendency to increase with q. Normalized distribution of ions calculated from the

last 20 ns of the simulation (Fig. S6c) shows that the ratio of free and bounded to the NP surface ions dramatically change with q. The interior of a nanoshell made of NPs carrying $q = 2e$ has a larger percentage of free ions (24.2 %) that are not adsorbed onto the NP surface than the nanoshells made from NP with $q = 4e$ (9.0 %) and $q = 8e$ (5.2 %), where ions are largely adsorbed on the shell surfaces. Importantly, nanoshells from NPs carrying $q = 2e$ have a larger cavity than the nanoshell from NPs carrying $q = 4e$, despite the stronger Coulombic repulsion between the NPs. The larger the charges on the NPs, the more counter ions need to enter the capsule interior to screen the NPs (double layer formation). These counter ions enter the capsule with their hydration layer and create osmotic pressure.[28] This process can be also seen as a buildup of pressure within submicron scale capsules.

Supplementary Video Files

Supplementary Movie 1

Three-dimensional reconstruction of the porous nanoshell with transmission electron microscopy tomography.

Supplementary Movie 2

Molecular dynamics simulation of a nanoshell in Model 2 carrying an effective charge of q = 2e. An atomistic representation shows the dynamics of individual CdS NPs and the hydroxyl-derived surface ligand groups on their surfaces. The view transitions to a surface representation which shows a cross-section view of the nanoshell and the movements of counter ions inside and outside of the nanoshell.

Supplementary Movie 3

Molecular dynamics simulation of a nanoshell in Model 3 carrying an effective charge of q = 0.6e. A surface representation shows the dynamical reorganization of bare CdS NP in explicit water solvent, leading to a more open porous structure from a closed shell structure.

References

1. MJ Frisch, GW Trucks, HB Schlegel, GE Scuseria, MA Robb, JR Cheeseman, G Scalmani, V Barone, B Mennucci, GA Petersson, H Nakatsuji, M Caricato, X Li, HP Hratchian, AF Izmaylov, J Bloino, G Zheng, JL Sonnenberg, M Hada, M Ehara, K Toyota, R Fukuda, J Haseg, D. F. Gaussian09, Revision B.01. *Gaussian Inc., Wallingford, CT* (2010).
2. Makino, K. & Ohshima, H. Electrophoretic mobility of a colloidal particle with constant surface charge density. *Langmuir* **26,** 18016–9 (2010).
3. Ufimtsev, I. S. & Martinez, T. J. Quantum Chemistry on Graphical Processing Units. 3. Analytical Energy Gradients, Geometry Optimization, and First Principles Molecular Dynamics. *J. Chem. Theory Comput.* **5,** 2619–28 (2009).
4. Sinyagin, A., Belov, A. & Kotov, N. A. Monte Carlo simulation of linear aggregate formation from CdTe nanoparticles. *Model. Simul. Mater. Sci. Eng.* **13,** 389–399 (2005).
5. Mikelonis, A. M., Youn, S. & Lawler, D. F. DLVO Approximation Methods for Predicting the Attachment of Silver Nanoparticles to Ceramic Membranes. *Langmuir* **32,** 1723–1731 (2016).
6. Petosa, A. R., Jaisi, D. P., Quevedo, I. R., Elimelech, M. & Tufenkji, N. Aggregation and deposition of engineered nanomaterials in aquatic environments: role of physicochemical interactions. *Environ. Sci. Technol.* **44,** 6532–49 (2010).
7. Hotze, E. M., Phenrat, T. & Lowry, G. V. Nanoparticle aggregation: challenges to understanding transport and reactivity in the environment. *J. Environ. Qual.* **39,** 1909–24
8. Hwang, G., Ahn, I.-S., Mhin, B. J. & Kim, J.-Y. Adhesion of nano-sized particles to the surface of bacteria: Mechanistic study with the extended DLVO theory. *Colloids Surfaces B Biointerfaces* **97,** 138–144 (2012).
9. Wijenayaka, L. A., Ivanov, M. R., Cheatum, C. M. & Haes, A. J. Improved Parametrization for Extended Derjaguin, Landau, Verwey, and Overbeek Predictions of Functionalized Gold Nanosphere Stability. (2015).
10. Tang, Z., Kotov, N. A. & Giersig, M. Spontaneous organization of single CdTe nanoparticles into luminescent nanowires. *Science.* **297,** 237–240 (2002).
11. Shanbhag, S. & Kotov, N. A. On the origin of a permanent dipole moment in nanocrystals with a cubic crystal lattice: effects of truncation, stabilizers, and medium for CdS tetrahedral homologues. *J. Phys. Chem. B* **110,** 12211–7 (2006).

12. Talapin, D. V., Shevchenko, E. V., Murray, C. B., Titov, A. V. & Král, P. Dipole - Dipole interactions in nanoparticle superlattices. *Nano Lett.* **7,** 1213–1219 (2007).

13. Kyrychenko, A., Karpushina, G. V., Bogatyrenko, S. I., Kryshtal, A. P. & Doroshenko, A. O. Preparation, structure, and a coarse-grained molecular dynamics model for dodecanethiol-stabilized gold nanoparticles. *Comput. Theor. Chem.* **977,** 34–39 (2011).

14. Auyeung, E. *et al.* DNA-mediated nanoparticle crystallization into Wulff polyhedra. *Nature* **505,** 73–7 (2014).

15. Tang, Z., Zhang, Z., Wang, Y., Glotzer, S. C. & Kotov, N. A. Self-assembly of CdTe nanocrystals into free-floating sheets. *Science.* **314,** 274–8 (2006).

16. Srivastava, S. *et al.* Light-controlled self-assembly of semiconductor nanoparticles into twisted ribbons. *Science* **327,** 1355–9 (2010).

17. Yeom, J. *et al.* Chiral templating of self-assembling nanostructures by circularly polarized light. *Nat. Mater.* **14,** 66–72 (2015).

18. Ascencio, J. A., Liu, H. B., Pal, U., Medina, A. & Wang, Z. L. Transmission electron microscopy and theoretical analysis of AuCu nanoparticles: Atomic distribution and dynamic behavior. *Microsc. Res. Tech.* **69,** 522–530 (2006).

19. Kyrychenko, A., Karpushina, G. V., Bogatyrenko, S. I., Kryshtal, A. P. & Doroshenko, A. O. Preparation, structure, and a coarse-grained molecular dynamics model for dodecanethiol-stabilized gold nanoparticles. *Comput. Theor. Chem.* **977,** 34–39 (2011).

20. Tang, D.-M. *et al.* Mechanical properties of Si nanowires as revealed by in situ transmission electron microscopy and molecular dynamics simulations. *Nano Lett.* **12,** 1898–904 (2012).

21. Fan, Z. *et al.* From sphere to multipod: thermally induced transitions of CdSe nanocrystals studied by molecular dynamics simulations. *J. Am. Chem. Soc.* **135,** 5869–76 (2013).

22. Auyeung, E. *et al.* DNA-mediated nanoparticle crystallization into Wulff polyhedra. *Nature* **505,** 73–77 (2013).

23. Xie, L. *et al.* Efficient amorphous platinum catalyst cluster growth on porous carbon: A combined molecular dynamics and experimental study. *Appl. Catal. B Environ.* **162,** 21–26 (2015).

24. Chen, C. *et al.* In-Situ High-Resolution Transmission Electron Microscopy Investigation of Overheating of Cu Nanoparticles. *Sci. Rep.* **6,** 19545 (2016).

25. Zhang, L. *et al.* Three-dimensional structural dynamics and fluctuations of DNA-nanogold conjugates by individual-particle electron tomography. *Nat. Commun.* **7,** 11083 (2016).

26. Chen, C. *et al.* In-Situ High-Resolution Transmission Electron Microscopy Investigation of Overheating of Cu Nanoparticles. *Sci. Rep.* **6,** 19545 (2016).

27. Silvera Batista, C. A., Larson, R. G. & Kotov, N. A. Nonadditivity of nanoparticle interactions. *Science.* **350,** 1242477–1242477 (2015).

28. Gao, C., Donath, E., Moya, S., Dudnik, V. & Möhwald, H. Elasticity of hollow polyelectrolyte capsules prepared by the layer-by-layer technique. *Eur. Phys. J. E* **5,** 21–27 (2001).